


FULL PAPER

Open Access



Concurrent effects of Martian topography on the thermosphere and ionosphere at high northern latitudes

Yiding Chen^{1,2,3,5*} , Libo Liu^{1,2,4,5}, Huijun Le^{1,2,4,5}, Hui Zhang^{1,2,4,5} and Ruilong Zhang^{1,2,4,5}

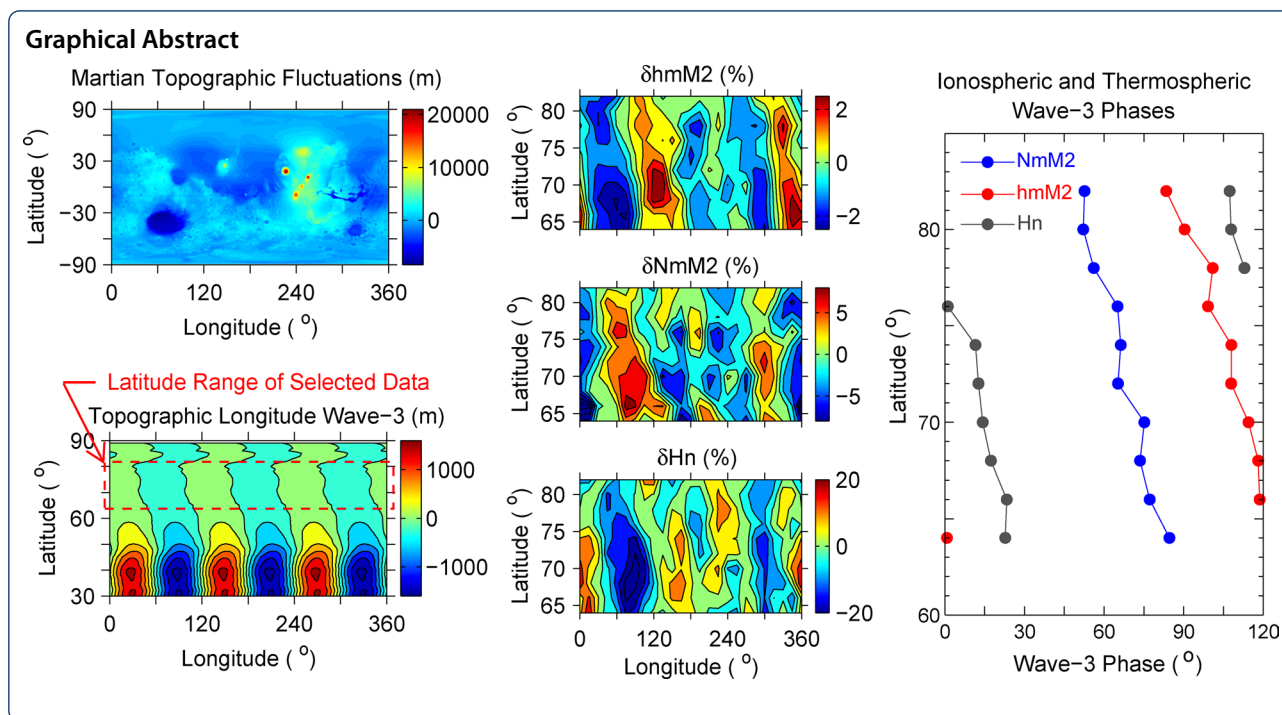
Abstract

Martian topography modulated non-migrating tides play important roles in the upper atmosphere and thus in the ionosphere through their coupling, especially in their longitude variations. In this study, the neutral scale height (H_n) and ionospheric peak electron density (N_mM_2) and height (h_mM_2) retrieved from the MGS radio occultation measurements were used to investigate the coupling between the Martian thermosphere and ionosphere under the forcing of topography modulated tides by investigating their concurrent longitude variations. A segment of the measurements with fixed local time was selected to analyze the relationships between the longitude variations of the parameters in detail. Longitude variations of the thermosphere and ionosphere are significant though topographic fluctuations are not very prominent at high northern latitudes. Longitude fluctuations of H_n and N_mM_2 are nearly in anti-phase and percentage fluctuation amplitudes of H_n are nearly twice as large as those of N_mM_2 , which indicate the non-migrating tide forced coupling between the ionosphere and thermosphere conforms to the Chapman theory, and suggests longitude variation of N_mM_2 can be used as a quantitative indicator for that of the thermal structure in the lower thermosphere. Longitude variation phases of H_n and h_mM_2 are also discrepant. That is due to tide vertical propagation since H_n and h_mM_2 depend on the atmospheric thermal structures at different height levels. The thermosphere and ionosphere show longitude variations due to the topography; however, they are dominated by inconsistent longitude components. This implies discrepant exciting and propagating efficiencies of various topography modulated tides.

Keywords: Martian ionosphere, Neutral scale height, Longitude variation

*Correspondence: chenyd@mail.iggcas.ac.cn

¹ Key Laboratory of Earth and Planetary Physics, Institute of Geology and Geophysics, Chinese Academy of Sciences, Beijing 100029, China
Full list of author information is available at the end of the article



Introduction

The solar-driven thermal tides play important roles in the variability and dynamics of the upper atmosphere of rapidly rotating planets such as the Earth and Mars; they transmit energy and momentum from the lower atmosphere to higher altitudes (e.g., Forbes et al. 2020; Moudén and Forbes 2008a). The thermal tides are westward propagating sun-synchronous waves when they are forced by zonally symmetrical solar heating (Chapman and Lindzen 1970), namely, migrating tides. Meanwhile, sun-asynchronous non-migrating tides are excited owing to the nonlinear modulation of zonal inhomogeneities near atmospheric lower boundary, such as topography, surface albedo, thermal inertia and so on (e.g., Withers et al. 2003), to the solar forcing. These non-migrating tides zonally propagate eastwards or westwards. Non-migrating tides were thought to be more important on Mars than on the Earth owing to the thinner atmosphere and much larger topographic fluctuations on Mars (e.g., Wang et al. 2006; Withers et al. 2003). They can significantly modulate Martian aerobraking region, and even may affect Martian atmosphere loss, known as the Jeans escape (e.g., Jakosky et al. 2015), if they propagate through the thermosphere to the exobase (Forbes et al. 2020). As the ionized part of the upper atmosphere, the ionosphere closely couples with the neutral atmosphere. Thus, non-migrating tides also can significantly modulate the Martian ionosphere (e.g., Bougher et al. 2001; Cahoy et al. 2007; Fang et al. 2021; Haider et al. 2011; Krymskii

et al. 2003, 2004; Mahajan et al. 2007; Thaller et al. 2020; Wang and Nielsen 2004; Withers 2009) through the coupling between the ionosphere and the upper atmosphere.

The influence of non-migrating tides on the Martian atmosphere manifests as planetary-scale longitude variations as seen from sun-synchronous orbits (fixed local times), where the influence of migrating tides is zonally symmetrical. The earlier knowledge on the longitude structures of the Martian upper atmosphere mainly came from accelerometer measurements. Keating et al. (1998) found a persistent zonal wave-2 structure in Martian atmospheric density based on the Mars Global Surveyor (MGS) accelerometer measurements; they suggested that the structure may be caused by a stationary planetary wave (SPW) associated with Martian topography. Subsequent analyses (e.g., Forbes and Zhang 2018; Wang et al. 2006; Wilson 2002) indicated there were significant differences in the longitude wave phase between different local solar times (LST), suggesting that upward propagating non-migrating tides are responsible for the wave structure. The in situ neutral density measurements from the recent Mars Atmosphere and Volatile Evolution (MAVEN) mission were also used to reveal the longitudinal wave structures associated with non-migrating tides in the upper atmosphere and their latitudinal and seasonal variations (e.g., England et al. 2016; Liu et al. 2017). Non-migrating tide propagation from the lower atmosphere into the thermosphere of Mars has been investigated by some simulations (e.g., Forbes et al. 2002;

Moudden and Forbes 2008b; Wilson 2002); whereas, vertical phase changes of the longitude structure were not clear in neutral density observations (e.g., Wang et al. 2006; Withers et al. 2003). Wave–wave interactions make tide propagation more complicated. Although SPWs excited in the lower atmosphere were generally not thought to be capable of propagating into the thermosphere, they can be generated by nonlinear wave–wave interactions in the upper atmosphere (e.g., Forbes et al. 2020).

Longitude variations of the Martian atmosphere were also revealed in its thermal structure that controls the variability of the upper atmosphere. Banfield et al. (2000) investigated the longitude waves in the thermal structure of the Martian atmosphere using the neutral temperature profiles retrieved from the thermal emission spectrometer on board the MGS. They extracted various migrating tides, non-migrating tides, and SPWs from the observations. Their results were mainly for the region below the thermosphere, the amplitudes of non-migrating tides were only on the order of ~ 1 K (the percentage with respect to zonal mean was $\sim 1\%$). Withers et al. (2011) showed the presence of atmospheric temperature longitude variations up to 110 km altitude using the measurements of the Spectroscopy for the Investigation of the Characteristics of the Atmosphere of Mars aboard Mars Express. In their results, the zonal temperature variations can reach the order of 10 K and wave – 2 and wave – 3 components are dominant. Recently, England et al. (2019) presented the longitude wave – 3 variations of neutral temperature in the upper thermosphere using the remote observations of the Imaging Ultraviolet Spectrograph aboard the MAVEN mission. Combining with the temperature measurements at lower altitudes by the Mars Reconnaissance Orbiter, they showed a phase shift with altitude in the wave – 3 component, indicating vertical wave propagation from the lower atmosphere to the upper atmosphere. Stevens et al. (2017) presented different longitude wave phases of atmospheric thermal structure between the mesosphere and the thermosphere.

Longitude variations associated with the non-migrating tides were also found in the Martian ionosphere. Bougher et al. (2001, 2004) showed a similar longitude variation profile of Martian dayside ionospheric peak height with that of the neutral density at 130 km height measured by the MGS. They suggested that ionospheric peak height can be used as a proxy of atmospheric longitude variations. Unlike ionospheric peak height, longitude variations of ionospheric peak electron density were not thought to be a primary effect of non-migrating tides since the electron density peaks occur near constant pressure levels (e.g., Mendillo et al. 2003; Rishbeth and Mendillo 2004); whereas, evident longitude variations

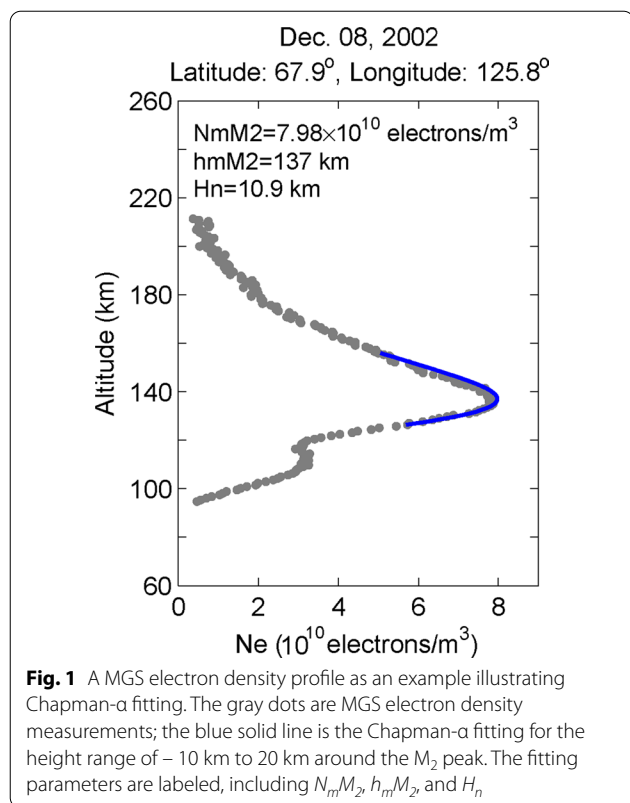
were also observed in the electron density (e.g., Cahoy et al. 2006, 2007; Haider et al. 2006; Krymskii et al. 2003; Mahajan et al. 2007). Cahoy et al. (2007) investigated longitude variations of ionospheric electron densities at different altitudes; they showed vertical phase change of the electron density longitude variations. Mahajan et al. (2007) showed that longitude variations of the height and density of the ionospheric peak are anticorrelated, which they characterized as an anomalous feature.

Therefore, although longitude variations of the thermosphere and the ionosphere have been presented, they are still deserving of further investigations, especially the relationship between them and how they couple under the forcing of non-migrating tides. This is the objective of this study. In “Data processing and results” section, data processing method of the MGS radio occultation electron density profiles is introduced and concurrent longitude variations of the thermosphere and ionosphere are presented. In “Discussion” section, the relationship between the observed thermospheric and ionospheric longitude variations and the topography is discussed, and the coupled responses of the thermosphere and ionosphere to the forcing of non-migrating tides are analyzed in terms of the Chapman theory. Finally, a summary is presented in “Summary” section.

Data processing and results

The MGS spacecraft launched in November 1996 arrived at Mars in September 1997. The spacecraft carried a radio occultation instrument that can measure Martian ionospheric electron density profiles. 5600 electron density profiles were obtained in total from the measurements during the MGS mission. This dataset has been well used to investigate Martian ionospheric variations (e.g., Bougher et al. 2001; Breus et al. 2004; Fox and Yeager 2009; Krymskii et al. 2003, 2004; Mahajan et al. 2007; Martinis et al. 2003; Mendillo et al. 2003; Rishbeth and Mendillo 2004; Zou et al. 2006, 2011).

Figure 1 shows a typical electron density profile of the Martian ionosphere measured by the MGS radio occultation as an example. The principal characteristic of the profile is the primary layer peaked at ~ 135 km, the M_2 layer. Below the M_2 layer there is a secondary layer peaked at ~ 110 km, the M_1 layer. The M_2 peak is always conspicuous in Martian dayside electron density profiles, while the M_1 peak is usually not obvious, instead often appearing as a shoulder (e.g., Fox and Yeager 2009). The M_2 peak is produced from the photoionization of CO_2 by solar extreme ultraviolet irradiance, in which the Helium-II 30.4 nm line is a major ionization source (e.g., Rishbeth and Mendillo 2004). The ionized CO_2^+ reacts with atomic oxygen so that the final dominant ion is the molecular ion O_2^+ in the vicinity of the M_2 peak. As a



result, variations of the electron density around the M_2 peak agree with those of a Chapman- α layer for which the neutral scale height is a crucial parameter (e.g., Fox and Yeager 2009; Mendillo et al. 2015; Rishbeth and Mendillo 2004; Sánchez-Cano et al. 2016). For a Chapman- α layer the altitudinal profile of the electron density can be described by the following Chapman- α function (for the M_2 layer):

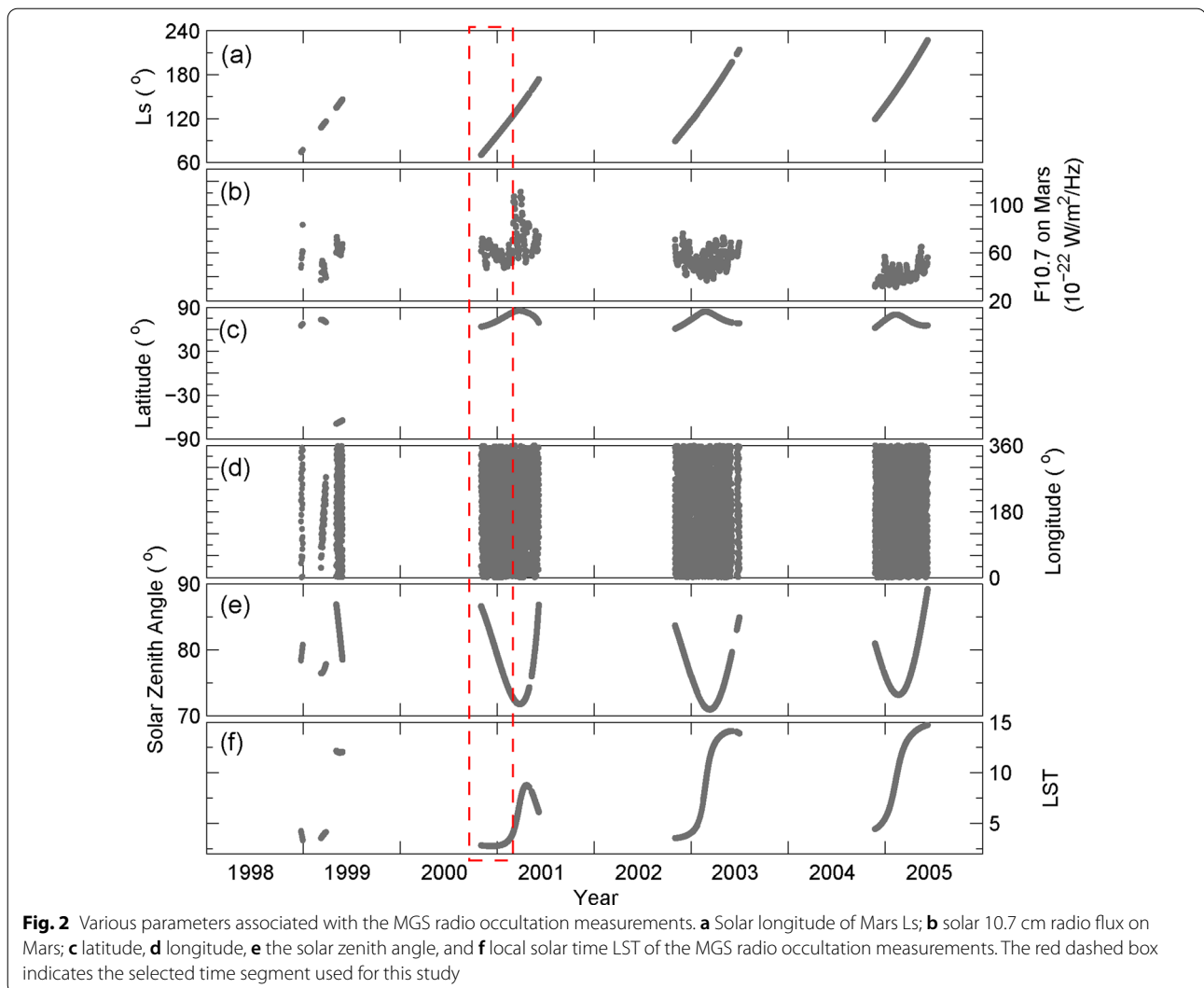
$$N_e(h) = N_m M_2 \cdot \exp \left[0.5 \cdot \left(1 - \frac{h - h_m M_2}{H_n} - e^{-\frac{h - h_m M_2}{H_n}} \right) \right], \quad (1)$$

where N_e is electron density, h is height, $N_m M_2$ is the peak electron density of the M_2 layer, $h_m M_2$ is the peak height of the M_2 layer, and H_n is the scale height of CO_2 . That is to say, the shape of the electron density profile strongly depends on H_n . The key parameters of the M_2 peak, $N_m M_2$ and $h_m M_2$, can be reliably identified from the electron density profiles recorded by the MGS radio occultation instrument, and the neutral scale height can be estimated by adjusting H_n to best fit those profiles using the Chapman- α function.

The ionization of atomic oxygen becomes important with increasing altitudes above the M_2 peak, and the ionization of CO_2 by solar X-ray gradually dominates the ionization rate with decreasing altitudes below the M_2

peak so that the M_1 layer forms. Thus, the Chapman- α function can only well describe the partial electron density profile in the vicinity of the M_2 peak. In this study, we used the Chapman- α function to fit the electron density profile within the altitudinal range of ~ 10 km to 20 km around the M_2 peak. This can avoid the lower M_1 layer and the higher M_2 topside. A 5-point running average was first applied to each electron density profile and the M_2 peak was identified from the profile to determine the fitting range. Then we applied the Chapman- α function to each profile to estimate the neutral scale height by adjusting H_n to best fit the electron density profile. In view of the uncertainties of the MGS measurements, the fitted $N_m M_2$ was also slightly adjusted (not exceed $\pm 2\%$) from the maximum electron density point recorded in the profile to achieve a best fitting. The typical uncertainty level of the MGS electron density is $\sim 3 \times 10^9 \text{ m}^{-3}$ as compared with a characteristic peak density of $\sim 80 \times 10^9 \text{ m}^{-3}$ observed at a solar zenith angle of 80° (Tyler et al. 2001), i.e., $\sim 3.8\%$. This adjustment does not exceed that uncertainty level. In Fig. 1, the blue solid line shows a Chapman- α fitting as an example. The fitting can well capture the partial electron density profile around the M_2 peak. H_n was determined by the fitting. The vast majority of the electron density profiles were well fitted. The fitting errors are well within the uncertainty level of the MGS electron density; the mean error is $1.70 \times 10^9 \text{ m}^{-3}$ and the standard deviation is $0.74 \times 10^9 \text{ m}^{-3}$.

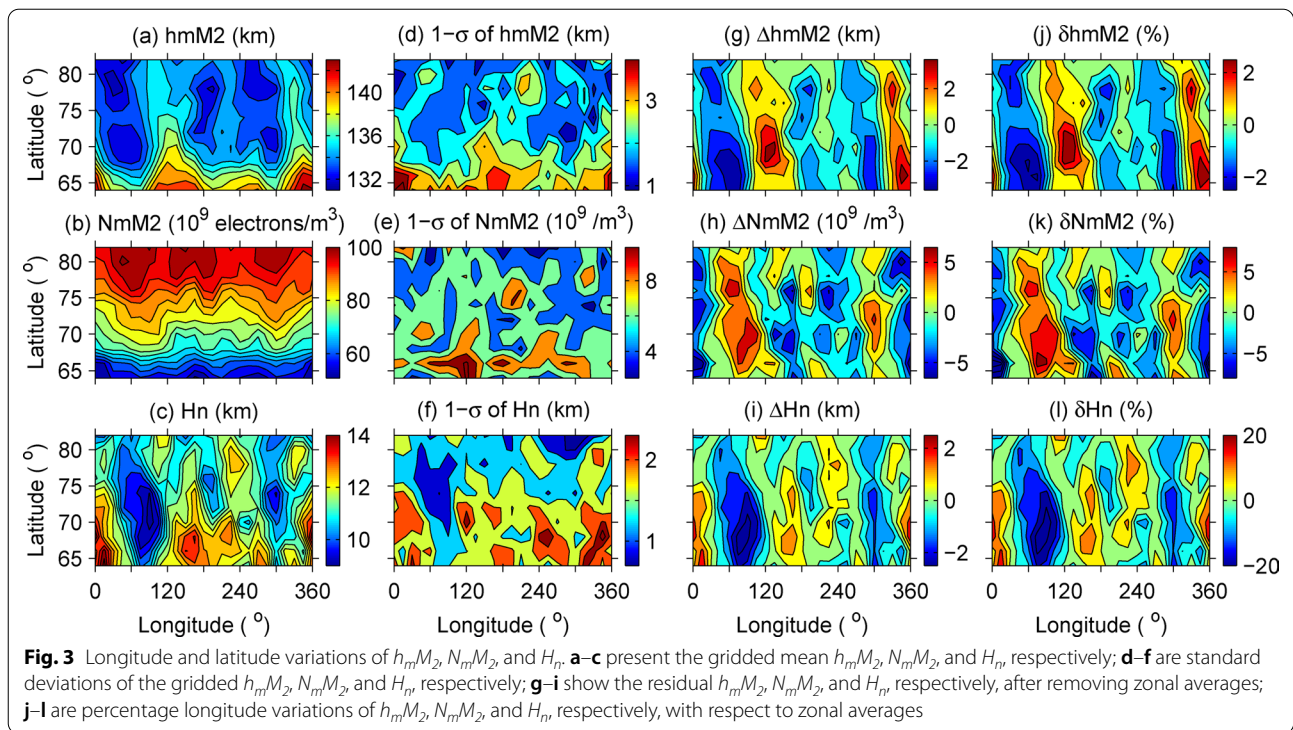
The objective of this study is to investigate the effects of Martian topography modulated tides on longitude variations of the ionosphere and thermosphere. The longitude difference of solar forcing to the ionosphere, which can be estimated by the solar zenith angle and solar irradiance flux, should be excluded for investigating ionospheric longitude variations. Moreover, the LST of the measurements should be fixed as possible owing to the propagating nature of non-migrating tides. Figure 2 shows solar longitude of Mars (Ls), solar 10.7 cm radio flux on Mars as well as latitude, longitude, the solar zenith angle, and LST of the MGS radio occultation measurements. All measurements occurred under the Martian seasonal condition of Ls is $\sim 70^\circ$ to $\sim 220^\circ$. The measurements were mainly confined to high northern latitudes and high solar zenith angles. Although the solar zenith angle changed with latitude, the measurements repeatedly covered the whole longitude range at different latitudes to ensure longitude variations of the parameters can be investigated. However, the measurements covered more than a half of the Solar Cycle 23 so that the solar flux changed significantly between different occultation seasons, and the LST of the measurements significantly changed during each occultation season. Thus, we selected an episode of the occultation season 2 in order



to reduce the effect of solar flux change and confine the LST range of the measurements. As indicated by the red box in Fig. 2, the measurements repeatedly covered different longitudes when the solar zenith angle decreased with increasing latitude, while the changes of solar flux and LST (confined to $LST \leq 04:00$) were smaller. That is to say, the solar forcing and the LST over different longitudes are basically equivalent at fixed latitudes so that the longitude variations associated with non-migrating tides can be retrieved.

We binned the data using a moving window of longitude $30^\circ \times$ latitude 4° with a step length of longitude $15^\circ \times$ latitude 2° to obtain gridded $h_m M_2$, $N_m M_2$, and H_n . The gridded data were further averaged to obtain mean longitude and latitude variations of the parameters, as shown in Fig. 3a–c. This is a smoothing operation combining measurements from different orbits to obtain average longitude variations of the parameters.

Figure 3d–f shows the corresponding standard deviations of the gridded $h_m M_2$, $N_m M_2$, and H_n , respectively. $h_m M_2$ decreases while $N_m M_2$ increases with increasing latitude owing to the solar zenith angle decreases with increasing latitude (see Fig. 1). Similar to $h_m M_2$, H_n tends to decrease with increasing latitude although the solar zenith angle decreases. This may be the manifestation of that neutral temperature decreases with decreasing altitude in the lower thermosphere. There are evident longitude fluctuations in the parameters, especially in $h_m M_2$ and H_n . The dominant longitude variation pattern is the 3-peak structure. In view of the background latitude variations of the parameters, we removed their longitudinal averages to more clearly present the longitude fluctuations, as shown in Fig. 3g–i. The mean longitude variations dominate over the standard deviations of the gridded data (Fig. 3d–f), indicating the significance of the mean longitude variations. For example, the mean longitude variation



of $h_m M_2$ can reach ~ 7 km, while the standard deviation of the gridded $h_m M_2$ is generally lower than ~ 4 km. The longitude fluctuation of $N_m M_2$ becomes clearer after removing the longitudinal averages. All parameters show significant 3-peak longitude structure. It is notable that the longitude variation phases of the parameters are inconsistent with each other and the amplitudes of the peaks are somewhat uneven. The percentage longitude variations of the parameters with respect to their zonal means were calculated, as shown in Fig. 3j–l. The percentage longitude variations of $h_m M_2$, $N_m M_2$, and H_n can reach the orders of $\sim 2\%$, $\sim 8\%$, and $\sim 20\%$, respectively.

A sixth-order Fourier decomposition was applied to the parameters' longitude fluctuations to further estimate the relative importance of various longitude variation components in more detail:

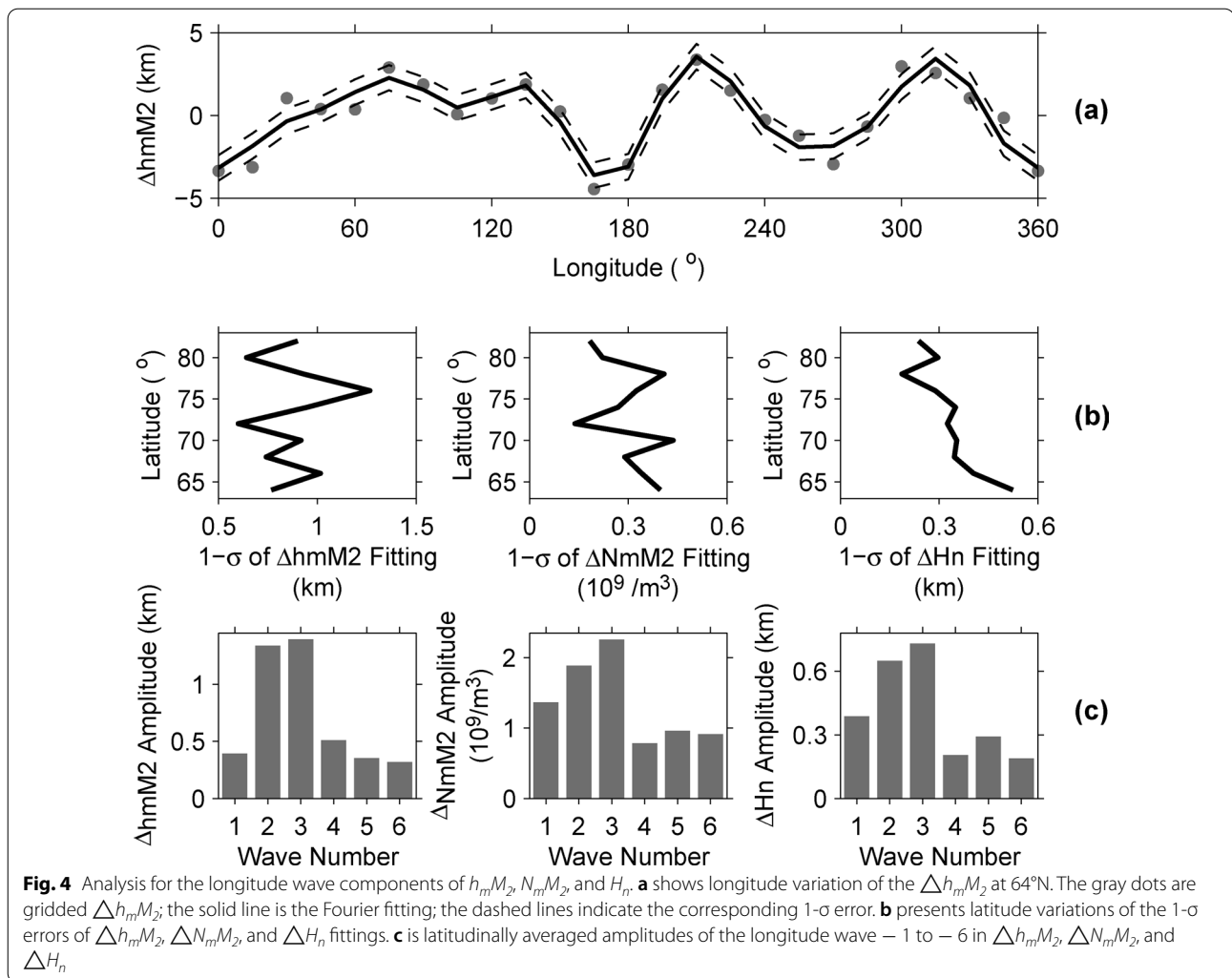
$$P_l(\lambda) = \sum_{n=1}^6 A_n \cos \left[\frac{2\pi n \cdot (\lambda - \psi_n)}{360} \right], \quad (2)$$

where λ is longitude, P_l is parameter's longitude fluctuation (Fig. 3g–i), and A_n and ψ_n are the amplitude and phase of wave- n component, respectively. Figure 4a shows the longitude variations of the $\Delta h_m M_2$ at $64^\circ N$ and its Fourier fitting to illustrate the decomposition. The solid line is the Fourier fitting; the dashed lines indicate the fitting error estimated by the standard deviation of the difference between the fitting and the observation.

The fitting can well capture the longitude variations, which significantly dominate over the fitting error. Thus, various wave amplitudes can be calculated from the fitting to estimate the relative importance of different wave components. Figure 4b presents the fitting errors of $\Delta h_m M_2$, $\Delta N_m M_2$, and ΔH_n , and Fig. 4c shows the latitudinally averaged amplitudes of the longitude wave-1 to -6 for the three parameters. The wave-2 and -3 are dominant longitude components; their amplitudes are significantly larger than the fitting errors. The wave-3 is somewhat higher in amplitude. The wave-3 corresponds to the conspicuous 3-peak structure in Fig. 3g–i, and the wave-2 can be used to explain the uneven amplitudes of the peaks. Moreover, the wave-1 is also important to some extent for $N_m M_2$ and H_n , which also can cause the uneven amplitudes of the peaks.

Discussion

The electron density profiles of the Martian dayside M_2 layer can be used to investigate the thermal structure of the lower thermosphere since they are dominated by photochemical processes. Krymskii et al. (2003, 2004) retrieved H_n from the MGS electron density profiles by assuming a parabolic electron density distribution in the vicinity of the M_2 peak; they showed the presence of H_n longitude variations. Zou et al. (2011) also estimated H_n from the MGS electron density profiles using the Taylor decomposition of the electron density with respect



to altitudes to analyze seasonal variations of the neutral atmosphere. In this study, we used a Chapman- α function that can well describe the electron density profiles of a photochemical equilibrium layer to estimate H_n . As shown in Fig. 3, the gridded mean H_n varies from ~ 9 km to ~ 14 km under the selected condition, basically consistent with the previous results (e.g., Krymskii et al. 2003, 2004; Zou et al. 2011).

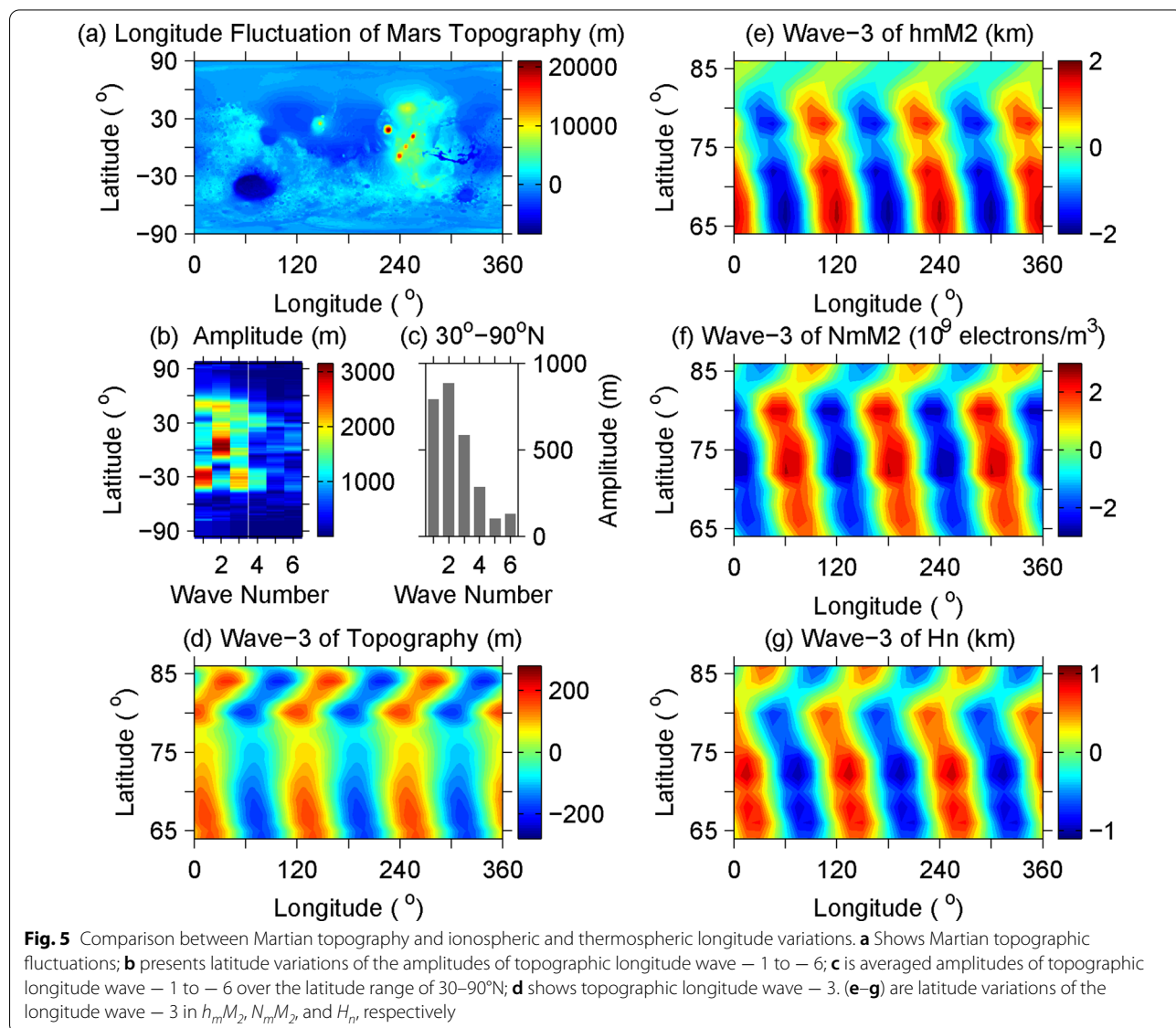
The amplitudes of thermal tides should increase with increasing altitudes according to the classical tidal theory (Chapman and Lindzen 1970); in contrast, the actual condition is that thermal tides undergo dissipation when propagating upwards (e.g., Withers et al. 2003). As shown in Fig. 3l, H_n longitude variations can reach $\sim 20\%$ in the lower thermosphere, which is much higher than the longitude variations of the neutral temperature at lower altitudes (e.g., Banfield et al. 2000). That is to say, tide wave amplitudes increase when propagating upwards into the lower thermosphere. For the ionosphere, Fang et al.

(2021) recently analyzed longitude variations of the ionospheric electron densities above the M_2 peak measured by the MAVEN mission. Their results indicated that longitude variation amplitudes of ionospheric electron density also trend to increase with increasing altitude; the longitude variations can reach $\sim 15\%$ near 200 km, significantly larger than the $\sim 8\%$ longitude variation of the electron density at the M_2 peak presented in this study. It is notable that Fang et al. (2021) showed that the amplitude of the wave-1 is comparable to those of the wave-2 and -3, which are two dominant longitude components in this study. This is possibly due to the different observational conditions and sampling modes of the two types of measurements, especially Fang et al. (2021) used the MAVEN measurements near 20°S while in this study we used the MGS measurements at high northern latitudes.

Topographic fluctuations are generally prominent on Mars, which were suggested to be the primary reason for atmospheric longitude variations (e.g., Forbes et al.

2002; Moudden and Forbes 2008b). Figure 5a shows Martian topography changes. The topography changes are much more significant at mid- and low-latitudes than at high latitudes; the most notable changes are two asymmetrical plateaus. Withers et al. (2003) and Moudden and Forbes (2008b) performed Fourier decompositions to the Martian topography and compared the decomposed zonal components with those of the MGS neutral density to relate atmospheric longitude variations to the topography. Their comparisons were for large latitudinal scales and indicated relevance between atmospheric longitude variations and the topography, with emphasis on low- and mid-latitudes. This study is confined to the longitude variations at high northern latitudes. The Fourier decomposition was also applied

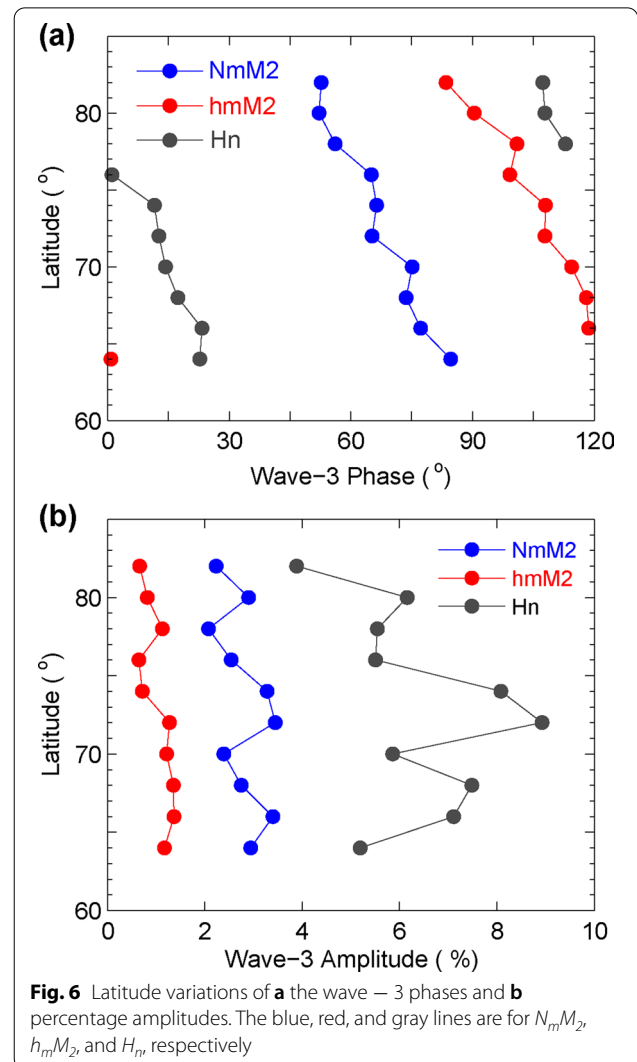
to the topography. As shown in Fig. 5b, the Fourier amplitudes of the longitude variations are significantly larger at low- and mid-latitudes than at high latitudes. The dominant longitude components include the wave - 1, - 2, and - 3, and the wave - 2 is more prominent in the northern hemisphere. The selected MGS radio occultation measurements are located at higher northern latitudes, as indicated by the red dashed box in Fig. 2. Figure 5c shows that the wave - 1, - 2, and - 3 are also dominant components at middle to high northern latitudes, and the mean amplitude of wave - 3 is somewhat lower than those of wave - 1 and - 2. Nonlinear modulation of topographic longitude wave-n to the solar forcing should induce apparent longitude wave-n variation in the atmosphere as seen at a fixed



LST (e.g., Forbes et al. 2002). That is to say, the topographic longitude components are not fully consistent with those of $h_m M_2$, $N_m M_2$, and H_n (Fig. 4), which mainly manifests as that a dominant longitude variation component in the topography, the wave - 1, is not prominent in $h_m M_2$, $N_m M_2$, and H_n . Then, what is the manifestation of the relevance between the ionospheric and thermospheric longitude structures and the topography in the selected data set? We took the dominant wave - 3 in the ionosphere and thermosphere to further analyze. A notable feature of the topographic wave- 3 is that the wave - 3 phase changes with latitude; it shifts westwards with increasing latitude in the latitudinal range of $\sim 50^\circ\text{N}$ to $\sim 80^\circ\text{N}$ and turns to shift eastwards beyond $\sim 80^\circ\text{N}$. Figure 5d presents the topographic wave - 3 in the latitudinal range of the MGS measurements to show these phase shifts. Latitude variations of the wave-3 in $h_m M_2$, $N_m M_2$, and H_n are presented in Fig. 5e-g, respectively, for comparison; where the data are extended to a larger LST range (LST < 6.7) to include those MGS measurements at higher latitudes to investigate the effect of the topographic wave - 3 phase turning at 80°N . It is interesting that similar phase shifts and turning appear in the three parameters, consistent with the topography. It is notable that the LST of the MGS measurements significantly increases with increasing latitude beyond $\sim 80^\circ\text{N}$ in the extended date set, which also contributes to the eastward wave - 3 phase shift in the MGS measurements at higher latitudes. The DE2 and SE1 tide components were suggested to be primarily responsible for the wave-3 longitude variations, and SE1 was thought to be more important at high latitudes (e.g., Cahoy et al. 2007; Forbes et al. 2002; Moulden and Forbes 2008b; Withers et al. 2003). Taking H_n for example, the wave-3 phase shifts eastwards $\sim 48^\circ$ from 80°N grid to 86°N grid. The calculated mean LST of the gridded data changes ~ 2.1 h from 80°N grid to 86°N grid, which corresponds to a wave-3 phase eastward shift of 10.5° (21°) for DE2 (SE1), significantly lower than the observed 48° phase shift. Thus, the observed turning of the phase shift at 80°N should be related to the topography. Based on simulations, Wilson (2002) also indicated westward phase shift of the wave-3 in neutral density with increasing latitude at high northern latitudes. The similar phase shifts in ionospheric and thermospheric longitude variations and in the topography indicate a commonality between them. Exciting and upward propagating efficiency may be different for various tide wave modes (e.g., Wang et al. 2006). Thus, the difference in the dominant longitude components between the three parameters and the topography is possibly

due to that various topography modulated wave modes have discrepant exciting and propagating efficiencies.

It is noticeable from Fig. 5e-g that the longitude variation phases of the three parameters are different from each other; especially the wave - 3 peaks of $N_m M_2$ are significantly asynchronous with those of $h_m M_2$ and H_n . Then, how do the ionosphere and thermosphere couple under the forcing of the topography modulated non-migrating tides? Fig. 6a further presents the wave-3 phases (ψ_3 in Eq. (2)) of $N_m M_2$, $h_m M_2$, and H_n for comparison. Differences between the phases are evident. Taking $N_m M_2$ for reference, the phase difference between $h_m M_2$ and $N_m M_2$ is $\sim 40^\circ$, and that between H_n and $N_m M_2$ is $\sim 60^\circ$, just a half of a wave-3 cycle (120° in longitude). Previous studies presented the phase discrepancies between the longitude variations of different neutral parameters. Withers et al. (2011) developed a formalism to explain the phase difference between



neutral temperature and atmospheric pressure, where the phase difference was attributed to the vertical change of the longitude variation amplitude of atmospheric pressure. England et al. (2019) presented the phase difference between the longitude variations of neutral temperature and atmospheric density. In this study, $N_{m}M_2$ primarily depends on the CO_2 density at h_mM_2 and H_n corresponds to the averaged neutral temperature in the vicinity of h_mM_2 , they are related to the state of the lower thermosphere at similar height levels. The ionization peak forms at the height where atmospheric optical depth [Eq. (3)] reaches one according to the Chapman theory that assumes the atmosphere is isothermal and horizontally stratified (Rishbeth and Garriott 1969):

$$\tau = \sigma n H_n \bullet \sec \chi, \quad (3)$$

where σ is absorption cross section, n is neutral density, and χ is the solar zenith angle. That means the ionization peak occurs at a constant atmospheric pressure level (Eq. (4)) for a fixed solar zenith angle:

$$P = nkT_n = nH_nmg, \quad (4)$$

where k is the Boltzmann constant, T_n is neutral temperature, m is molecular mass, and g is the gravity acceleration. Simulations (González-Galindo et al. 2013) showed that the Martian M_2 peak at the subsolar point is nearly located at the same atmospheric pressure level through a Martian year. Thus, $N_{m}M_2$ variation should be negatively correlated with H_n variation in view of that $N_{m}M_2$ is positively correlated with n . That means longitude variations of $N_{m}M_2$ and H_n should be in anti-phase, just as presented in Fig. 6a. This result indicates that longitude variations of H_n driven by non-migrating tides modulate the concurrent longitude variations of $N_{m}M_2$ according to the Chapman theory, although the Martian atmosphere is longitudinally varying and is not strictly isothermal (the neutral temperature in the lower thermosphere can increase by tens of Kelvin from ~ 120 km to ~ 160 km, e.g., Cui et al. 2018; Fox et al. 1996; Mendillo et al. 2011).

h_mM_2 is positively correlated with the neutral scale height according to the Chapman theory (Rishbeth and Garriott 1969). Longitude variations of the ionosphere can be attributed to those of H_n , then longitude variations of h_mM_2 should be in-phase with those of H_n . However, they are also not in-phase in observations (see Figs. 3 and 6a). The atmospheric optical depth increases with decreasing altitude, and for an ionization layer dominated by photochemical processes, h_mM_2 corresponds to the height where the atmospheric optical depth equal to one. The atmospheric optical depth is related to the column content of ionized neutral composition downward from atmospheric top. The atmospheric column content depends on the underlying atmospheric temperature,

which determines the expansion or contraction of the overlying atmosphere (e.g., Bougher et al. 2001; Zou et al. 2011; González-Galindo et al. 2013). Thus, h_mM_2 mainly depends on the neutral temperature below the M_2 peak, which controls the atmospheric column content above the M_2 peak. For the actual Martian atmosphere (in which neutral temperature changes with increasing altitudes), this neutral temperature should be the effective one of the underlying atmosphere mostly lower than h_mM_2 , as revealed by Zou et al. (2011) that the effective neutral scale height between the lower atmosphere and the ionospheric peak is the primary driver for h_mM_2 variations. That means the height level of the atmospheric temperature determining h_mM_2 is lower than the height level of H_n . Thus, the difference of the wave -3 phase between h_mM_2 and H_n indicates vertical change of the longitude variation phase of neutral temperature. Although both SPWs, which can be generated from non-linear atmospheric wave-wave interactions (e.g., Forbes et al. 2020), and non-migrating tides can cause atmospheric longitude variations, the observed wave phases of the thermosphere and ionosphere under the selected condition is consistent with vertical non-migrating tide propagation, since the wave -3 of h_mM_2 should be in-phase with that of H_n if the longitude variations are caused by SPWs (their phases keep constant with varying altitude).

The percentage magnitudes of the longitude variations of the parameters also differ from each other, as presented in Fig. 3j–l. Figure 6b further shows the wave-3 percentage amplitudes [A_3 in Eq. (2)] of $N_{m}M_2$, h_mM_2 , and H_n for comparison. The percentage amplitudes of H_n are nearly twice as large as those of $N_{m}M_2$. The latitudinally averaged ratio of H_n amplitudes to $N_{m}M_2$ amplitudes is ~ 2.3 , similar to the ratio of their total longitude variation magnitudes (Fig. 3). For a Chapman- α layer $N_{m}M_2$ is proportional to $H_n^{-1/2}$, which means a change of the neutral scale height $\Delta H_n/H_n$ will cause a smaller change of the electron density $\Delta N_{m}M_2/N_{m}M_2$ with a magnitude of half that of $\Delta H_n/H_n$. Thus, the wave-3 amplitude ratio of H_n to $N_{m}M_2$ is basically consistent with the Chapman- α layer. A possible reason for the smaller difference is that the mean height of the altitudinal range (-10 km to 20 km around h_mM_2) used for fitting H_n is higher than h_mM_2 . The percentage amplitudes of the longitude variations of h_mM_2 are much smaller than those of H_n , h_mM_2 linearly depends on the neutral scale height according to the Chapman theory:

$$h_mM_2(\chi) = h_mM_2(\chi = 0) + H_n' \bullet \ln(\sec \chi), \quad (5)$$

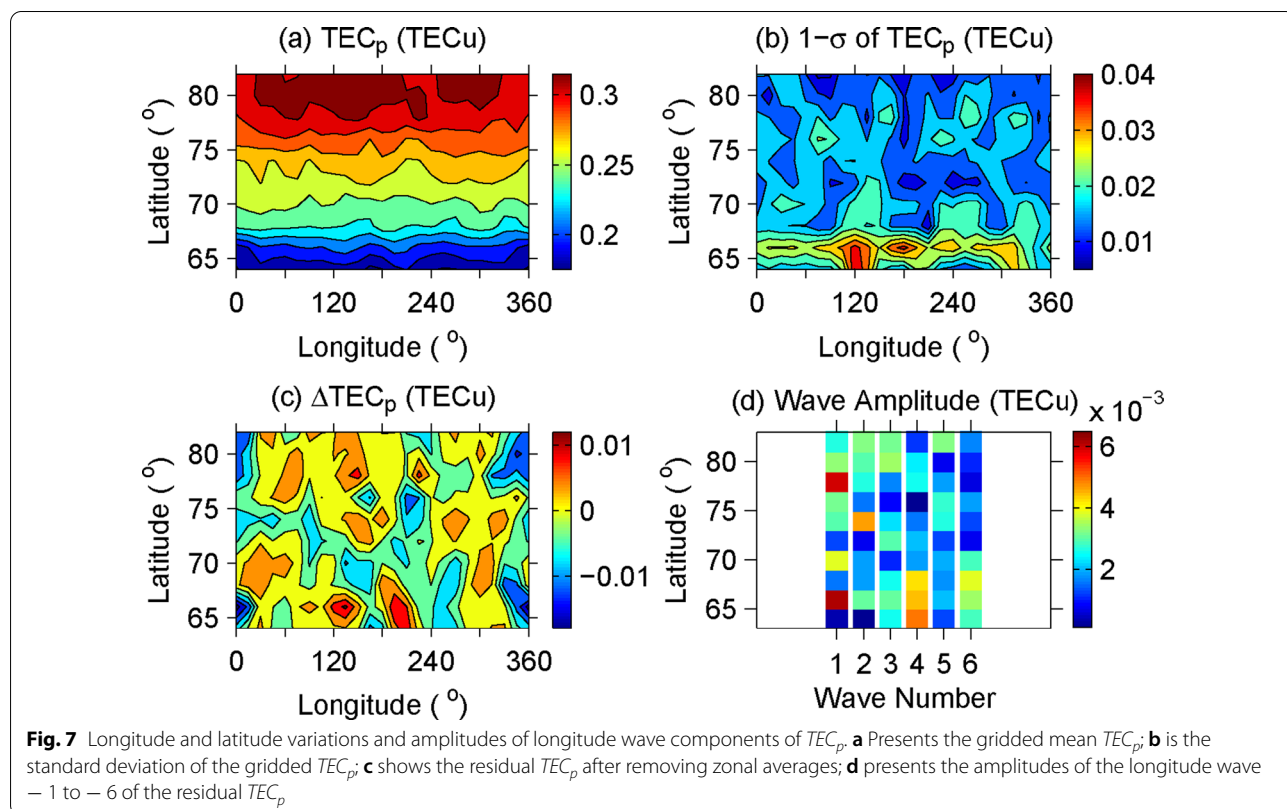
where χ is the solar zenith angle; in view of the vertical changes of neutral temperature, H_n' is the effective

neutral scale height of the atmosphere below the M_2 peak. Since the value of $h_{nr}M_2$ is dominated by the base value of $\chi=0$ (e.g., Morgan et al. 2008), the percentage variation of $h_{nr}M_2$ caused by the change of the neutral scale height is much smaller than that of the neutral scale height.

The observed wave phases of H_n and $h_{nr}M_2$ indicate the presence of the effect of upward propagating non-migrating tides, which is consistent with Cahoy et al. (2007), who presented vertical phase shifts of ionospheric longitude waves using the MGS electron density profiles. Owing to the vertical change of wave phase associated with tides, the dominant longitude variations should be weakened when integrating the electron densities with respect to altitudes, since out-of-phase longitude variations of the electron densities at different altitudes counteract partially. Thus, we calculated the total electron content of partial M_2 layer (TEC_p , in units of TECu, $1\text{TECu}=10^{16}$ electrons/m²) to investigate its longitude variations. In view of $h_{nr}M_2$ varies with longitude and latitude under the selected condition (see Fig. 3), for each electron density profile a TEC_p value was obtained by integrating the electron densities in the altitudinal range of -15 km to 25 km around the M_2 peak, where a main portion of the M_2 layer locates. TEC_p data were also gridded according to the operation used in Fig. 3.

Figure 7a shows longitude and latitude variations of the gridded mean TEC_p and Fig. 7b presents the corresponding standard deviations of the gridded TEC_p . TEC_p varies primarily with latitude due to the change of the solar zenith angle, which is similar to $N_{nr}M_2$ (see Fig. 3), while its longitude variation appears to be not as evident as that in $N_{nr}M_2$. Figure 7c presents the longitude variation using the residual TEC_p after removing zonal averages (ΔTEC_p). As expected, the aforementioned wave -3 and -2 are not evident in ΔTEC_p , and the longitude variation of ΔTEC_p is basically equivalent to the standard deviation of the gridded TEC_p in amplitude. Figure 7d further shows the amplitudes of the longitude wave -1 to -6 of ΔTEC_p . There is seems no a wave component that can be dominant at different latitudes. The amplitudes of others wave components can be comparable to those of wave -3 and -2 . Thus, the analysis for ΔTEC_p further supports that ionospheric longitude variations are related to upward propagating non-migrating tides.

The above analyses indicate that the observed ionospheric longitude variations are the results of the coupling between the ionosphere and thermosphere through photochemical processes under the forcing of topography modulated thermal tides. For this coupling, the neutral scale height is the key atmospheric parameter determining ionospheric longitude variations. The relationship



between ionospheric and thermospheric longitude variations conforms to the Chapman theory and vertical propagation of non-migrating thermal tides. The results suggest that longitude variation of $N_m M_2$ can be used as a quantitative indicator for that of the thermal structure in the lower thermosphere (for both amplitude and phase).

Summary

In this study, H_n of the Martian lower thermosphere was retrieved from the MGS electron density profiles, then concurrent longitude variations in the Martian ionosphere and lower thermosphere at high northern latitudes were investigated using $h_m M_2$, $N_m M_2$, and H_n . The data during a period with small LST changes were used such that longitude variations associated with topography modulated non-migrating tides can be analyzed in detail. Longitude variations of H_n , $N_m M_2$ and $h_m M_2$ can reach $\sim 20\%$, $\sim 8\%$ and $\sim 2\%$, respectively. The thermosphere and the ionosphere have similar longitude components dominated by the wave -3 and -2 ; however, these components are not fully consistent with those of the topography, in which the wave -1 is also dominant. Moreover, longitude variations of the three parameters are different from each other.

The dominant wave -3 was further analyzed in detail. Longitude variations of the ionosphere and thermosphere show evident relevance to the topography. With increasing latitudes, the wave phases of the thermosphere and ionosphere show similar westward shifts with that of the topography. Thus, the different longitude components of the ionosphere and thermosphere from those of the topography imply discrepant exciting and propagating efficiencies of various topography modulated waves. Ionospheric longitude variations form as the result of the coupling between the ionosphere and the thermosphere; for this coupling the neutral scale height is the key atmospheric parameter determining ionospheric longitude variations. Both the wave-3 phases and percentage amplitudes of $h_m M_2$, $N_m M_2$, and H_n are different from each other. The phase difference between H_n and $N_m M_2$ is about a half of a wave cycle, and the amplitudes of H_n are nearly twice as large as those of $N_m M_2$. Both are consistent with the Chapman theory. The much smaller amplitudes of $h_m M_2$ than those of H_n are also in line with the Chapman theory. Moreover, the phase difference between H_n and $h_m M_2$ can be attributed to the vertical propagation of atmospheric thermal tides, since H_n and $h_m M_2$ depend on the neutral temperatures at different height levels.

Abbreviations

H_n : Neutral scale height; $N_m M_2$: Peak electron density of the M_2 layer; $h_m M_2$: Peak height of the M_2 layer; MGS: Mars Global Surveyor; SPW: Stationary

Planetary Wave; LST: Local Solar Time; Ls: Solar longitude of Mars; TEC_p : Total Electron Content of partial M_2 layer.

Acknowledgements

The authors thank the MGS Radio Science Team for making the ionospheric electron density profile data and the MGS MOLA Science Team for producing the Martian topography data.

Authors' contributions

YC performed the data analyses and wrote the manuscript. LL, HL, HZ and RZ participated in the discussion for the results and revised the manuscript. All authors read and approved the final manuscript.

Funding

This research was supported by the Strategic Priority Research Program of Chinese Academy of Sciences (Grant No. XDB 41000000), National Natural Science Foundation of China (41922029, 42030202), and Youth Innovation Promotion Association, CAS (Grant No. Y202021).

Availability of data and materials

The MGS electron density profiles are available at <https://pds-ppi.igpp.ucla.edu/search/?sc=Mars+Global+Surveyor&t=Mars&i=RSS>; the Martian topography data can be obtained from <https://pds-geosciences.wustl.edu/missions/mgs/mola.html>.

Declarations

Competing interests

The authors declare that they have no competing interests.

Author details

¹Key Laboratory of Earth and Planetary Physics, Institute of Geology and Geophysics, Chinese Academy of Sciences, Beijing 100029, China. ²Innovation Academy for Earth Science, CAS, Beijing 100029, China. ³Beijing National Observatory of Space Environment, Institute of Geology and Geophysics, Chinese Academy of Sciences, Beijing 100029, China. ⁴Heilongjiang Mohe Observatory of Geophysics, Institute of Geology and Geophysics, Chinese Academy of Sciences, Beijing 100029, China. ⁵College of Earth and Planetary Sciences, University of Chinese Academy of Sciences, Beijing 100049, China.

Received: 7 September 2021 Accepted: 19 January 2022

Published online: 09 February 2022

References

- Banfield D, Conrath B, Pearl JC, Smith MD, Christensen P (2000) Thermal tides and stationary waves on Mars as revealed by Mars Global Surveyor thermal emission spectrometer. *J Geophys Res* 105:9521–9537
- Bougher SW, Engel S, Hinson DP, Forbes JM (2001) Mars Global Surveyor Radio Science electron density profiles: neutral atmosphere implications. *Geophys Res Lett* 28:3091–3094
- Bougher SW, Engel S, Hinson DP, Murphy JR (2004) MGS Radio Science electron density profiles: interannual variability and implications for the Martian neutral atmosphere. *J Geophys Res* 109:E03010. <https://doi.org/10.1029/2003JE002154>
- Breus TK, Krymskii AM, Crider DH, Ness NF, Hinson D, Barashyan KK (2004) Effect of the solar radiation in the topside atmosphere/ionosphere of Mars: Mars Global Surveyor observations. *J Geophys Res* 109:A09310. <https://doi.org/10.1029/2004JA010431>
- Cahoy KL, Hinson DP, Tyler GL (2006) Radio science measurements of atmospheric refractivity with Mars Global Surveyor. *J Geophys Res* 111:E05003. <https://doi.org/10.1029/2005JE002634>
- Cahoy KL, Hinson DP, Tyler GL (2007) Characterization of a semidiurnal eastward-propagating tide at high northern latitudes with Mars Global Surveyor electron density profiles. *Geophys Res Lett* 34:L15201. <https://doi.org/10.1029/2007GL030449>
- Chapman S, Lindzen RS (1970) Atmospheric tides. Springer, New York
- Cui J, Yelle RV, Zhao L-L, Stone S, Jiang F-Y, Cao Y-T, Yao M-J, Koskinen TT, Wei Y (2018) The impact of crustal magnetic fields on the thermal structure of

- the Martian Upper Atmosphere. *Astrophys J* 853:L33. <https://doi.org/10.3847/2041-8213/aaa89a>
- England SL, Liu G, Withers P, Yiğit E, Lo D, Jain S et al (2016) Simultaneous observations of atmospheric tides from combined in situ and remote observations at Mars from the MAVEN spacecraft. *J Geophys Res* 121:594–607. <https://doi.org/10.1002/2016JE004997>
- England SL, Liu G, Kumar A, Mahaffy PR, Elrod M, Benna M et al (2019) Atmospheric tides at high latitudes in the Martian upper atmosphere observed by MAVEN and MRO. *J Geophys Res* 124:2943–2953. <https://doi.org/10.1029/2019JA026601>
- Fang X, Forbes JM, Gan Q, Liu G, Thaller S, Bougher S et al (2021) Tidal effects on the longitudinal structures of the Martian thermosphere and topside ionosphere observed by MAVEN. *J Geophys Res* 126:e2020JA028562. <https://doi.org/10.1029/2020JA028562>
- Forbes JM, Zhang X (2018) Polar region variability in the lower thermosphere of Mars from odyssey and reconnaissance orbiter aerobraking measurements. *J Geophys Res* 123:8664–8687. <https://doi.org/10.1029/2018JG025527>
- Forbes JM, Bridger AFC, Bougher SW, Hagan ME, Hollingsworth JL, Keating GM, Murphy J (2002) Nonmigrating tides in the thermosphere of Mars. *J Geophys Res* 107:5113. <https://doi.org/10.1029/2001JE001582>
- Forbes JM, Zhang X, Forget F, Millour E, Kleinböhl A (2020) Solar tides in the middle and upper atmosphere of Mars. *J Geophys Res* 125:e2020JA028140. <https://doi.org/10.1029/2020JA028140>
- Fox JL, Yeager KE (2009) MGS electron density profiles: analysis of the peak magnitudes. *Icarus* 200:468–479. <https://doi.org/10.1016/j.icarus.2008.12.002>
- Fox JL, Zhou P, Bougher SW (1996) The Martian thermosphere/ionosphere at high and low solar activities. *Adv Space Res* 17:203–218
- González-Galindo F, Chaufray J-Y, López-Valverde MA, Gilli G, Forget F, Leblanc F, Modolo R, Hess S, Yagi M (2013) Three-dimensional Martian ionosphere model: I. The photochemical ionosphere below 180 km. *J Geophys Res* 118:2105–2123. <https://doi.org/10.1002/jgre.20150>
- Haider SA, Seth SP, Choksi VR, Oyama KI (2006) Model of photoelectron impact ionization within the high latitude ionosphere at Mars: comparison of calculated and measured electron density. *Icarus* 185:102–112
- Haider SA, Mahajan KK, Kallio E (2011) Mars ionosphere: a review of experimental results and modeling studies. *Rev Geophys* 49:RG4001. <https://doi.org/10.1029/2011RG000357>
- Jakosky BM, Lin RP, Grebowsky JM, Luhmann JG, Mitchell DF, Beutelschies G et al (2015) The Mars atmosphere and volatile evolution (MAVEN) mission. *Space Sci Rev* 195:3–48. <https://doi.org/10.1007/s11214-015-0139-x>
- Keating GM, Bougher SW, Zurek RW, Tolson RH, Cancro GJ, Noll SN et al (1998) The structure of the upper atmosphere of Mars: in situ accelerometer measurements from Mars Global Surveyor. *Science* 279:1672–1676
- Krymskii AM, Breus TK, Ness NF, Hinson DP, Bojkov DI (2003) Effect of crustal magnetic fields on the near terminator ionosphere at Mars: comparison of in situ magnetic field measurements with the data of radio science experiments on board Mars Global Surveyor. *J Geophys Res* 108:1431. <https://doi.org/10.1029/2002JA009662>
- Krymskii AM, Ness NF, Crider DH, Breus TK, Acuña MH, Hinson DP (2004) Solar wind interaction with the ionosphere/atmosphere and crustal magnetic fields at Mars: Mars Global Surveyor Magnetometer/Electron Reflectometer, radio science, and accelerometer data. *J Geophys Res* 109:A11306. <https://doi.org/10.1029/2004JA010420>
- Liu G, England S, Lillis RJ, Mahaffy PR, Elrod M, Benna M, Jakosky B (2017) Longitudinal structures in Mars' upper atmosphere as observed by MAVEN/NGIMS. *J Geophys Res* 122:1258–1268. <https://doi.org/10.1002/2016JA023455>
- Mahajan KK, Singh S, Kumar A, Raghuvanshi S, Haider SA (2007) Mars Global Surveyor radio science electron density profiles: some anomalous features in the Martian ionosphere. *J Geophys Res* 112:E10006. <https://doi.org/10.1029/2006JE002876>
- Martinis CR, Wilson JK, Mendillo MJ (2003) Modeling day-to-day ionospheric variability on Mars. *J Geophys Res* 108:1383. <https://doi.org/10.1029/2003JA009973>
- Mendillo M, Smith S, Wroten J, Rishbeth H, Hinson D (2003) Simultaneous ionospheric variability on Earth and Mars. *J Geophys Res* 108:1432. <https://doi.org/10.1029/2003JA009961>
- Mendillo M, Lollo A, Withers P, Matta M, Pätzold M, Tellmann S (2011) Modeling Mars' ionosphere with constraints from same-day observations by Mars Global Surveyor and Mars Express. *J Geophys Res* 116:A11303. <https://doi.org/10.1029/2011JA016865>
- Mendillo M, Narvaez C, Matta M, Vogt M, Mahaffy P, Benna M, Jakosky B (2015) MAVEN and the Mars Initial Reference Ionosphere model. *Geophys Res Lett* 42:9080–9086. <https://doi.org/10.1002/2015GL065732>
- Morgan DD, Gurnett DA, Kirchner DL, Fox JL, Nielsen E, Plaut JJ (2008) Variation of the Martian ionospheric electron density from Mars Express radar soundings. *J Geophys Res* 113:A09303. <https://doi.org/10.1029/2008JA013313>
- Moudden Y, Forbes JM (2008a) Effects of vertically propagating thermal tides on the mean structure and dynamics of Mars' lower thermosphere. *Geophys Res Lett* 35:L23805. <https://doi.org/10.1029/2008GL036086>
- Moudden Y, Forbes JM (2008b) Topographic connections with density waves in Mars' aerobraking regime. *J Geophys Res* 113:E11009. <https://doi.org/10.1029/2008JE003107>
- Rishbeth H, Garriott OK (1969) Introduction to ionospheric physics. Elsevier, New York
- Rishbeth H, Mendillo M (2004) Ionospheric layers of Mars and Earth. *Planet Space Sci* 52:849–852
- Sánchez-Cano B, Lester M, Witasse O, Milan SE, Hall BES, Cartacci M et al (2016) Solar cycle variations in the ionosphere of Mars as seen by multiple Mars Express data sets. *J Geophys Res* 121:2547–2568. <https://doi.org/10.1002/2015JA022281>
- Stevens MH, Siskind DE, Evans JS, Jain SK, Schneider NM, Deighan J et al (2017) Martian mesospheric cloud observations by IUVS on MAVEN: thermal tides coupled to the upper atmosphere. *Geophys Res Lett* 44:4709–4715. <https://doi.org/10.1002/2017GL072717>
- Thaller SA, Andersson L, Pilinski MD, Thiemann E, Withers P, Elrod M et al (2020) Tidal wave-driven variability in the Mars ionosphere-thermosphere system. *Atmosphere* 11:521. <https://doi.org/10.3390/atmos11050521>
- Tyler GL, Balmino G, Hinson DP, Sjogren WL, Smith DE, Simpson RA, Asmar SW, Priest P, Twicken JD (2001) Radio science observations with Mars Global Surveyor: Orbit insertion through one Mars year in mapping orbit. *J Geophys Res* 106:23327–23348. <https://doi.org/10.1029/2000JE001348>
- Wang J-S, Nielsen E (2004) Evidence for topographic effects on the Martian ionosphere. *Planet Space Sci* 52:881–886. <https://doi.org/10.1016/j.pss.2004.01.008>
- Wang L, Fritts DC, Tolson RH (2006) Nonmigrating tides inferred from the Mars Odyssey and Mars Global Surveyor aerobraking data. *Geophys Res Lett* 33:L23201. <https://doi.org/10.1029/2006GL027753>
- Wilson RJ (2002) Evidence for non-migrating thermal tides in the Mars upper atmosphere from the Mars Global Surveyor Accelerometer Experiment. *Geophys Res Lett* 29:1120. <https://doi.org/10.1029/2001GL013975>
- Withers P (2009) A review of observed variability in the dayside ionosphere of Mars. *Adv Space Res* 44:277–307
- Withers P, Bougher SW, Keating GM (2003) The effects of topographically-controlled thermal tides in the martian upper atmosphere as seen by the MGS accelerometer. *Icarus* 164:14–32
- Withers P, Pratt R, Bertaux J-L, Montmessin F (2011) Observations of thermal tides in the middle atmosphere of Mars by the SPICAM instrument. *Adv Space Res* 116:E11005. <https://doi.org/10.1029/2011JE003847>
- Zou H, Wang J-S, Nielsen E (2006) Reevaluating the relationship between the Martian ionospheric peak density and the solar radiation. *Adv Space Res* 111:A07305. <https://doi.org/10.1029/2005JA011580>
- Zou H, Lillis RJ, Wang J-S, Nielsen E (2011) Determination of seasonal variations in the Martian neutral atmosphere from observations of ionospheric peak height. *Adv Space Res* 116:E09004. <https://doi.org/10.1029/2011JG003833>

Publisher's Note

Springer Nature remains neutral with regard to jurisdictional claims in published maps and institutional affiliations.